RESEARCH ARTICLE

Editor's Choice

ADVANCED MATERIALS INTERFACES

www.advmatinterfaces.de

One-Step Bottom-Up Growth of Highly Liquid Repellent Worm-Like Surfaces on Planar Substrates

*Zhengtao Chen, Tien H. Nguyen, Shayna M. Rumrill, and Kenneth K. S. Lau**

Highly liquid repellent (superhydrophobic, superoleophobic) surfaces are fabricated using mostly top-down approaches and liquid-based processing. Top-down approaches, like lithography and templating, are highly process-intensive, while liquid-based processing, like etching and fluoropolymer solution coating, rely on solvents that often damage the substrate. Ultimately, to suppress liquids from spreading, the goal is to create a surface with low surface energy and a hierarchically roughened topology. Here, a bottom-up approach that achieves these two prerequisite criteria in one single step is demonstrated. Relying on a liquid-free initiated chemical vapor deposition (iCVD) process, worm-like protrusions of a semicrystalline fluoropolymer (poly(perfluorodecyl acrylate)) directly grow on flat substrates without prior surface pretreatment. The nano/microworm surfaces display super-liquid repellency (>150° contact angle) to water and oil. Worm formation (as opposed to conformal thin film formation) is attributed to preferential crystal nucleation, orientation, and growth on the substrate plane.

1. Introduction

Liquid repellent surfaces are often found in nature. For example, the lotus leaf surface is well-known for its superhydrophobic and self-cleaning properties that allow water droplets to easily roll off and pick up dirt particles along the way. Its water repellency comes from its unique low surface energy microrelief structure created by the papillose epidermal cells with epicuticular wax crystals that form over the surface.[1] Oil repellency in air, although more rare, is also observed in nature, like on a springtail's skin.[2] The skin is packed with bristles capped with rhombic meshes of nanogranules, a type of re-entrant structure that is key to achieving superoleophobicity.[3,4] Such liquid repellent structures have been imitated, studied experimentally, and described theoretically in the past several decades.[5–11] It is generally understood that surfaces need to have micro- and nanorelief structures, which deter liquids from spreading and wetting, in order to create superhydrophobicity or superoleophobicity, where the water or oil contact angle is larger than 150°, respectively. In some cases, surfaces can display both high water and oil repellency simultaneously, which are known as superomniphobic surfaces. Super liquid repellent coatings and surfaces are useful in a broad range of applications, including self-cleaning,[12] water-oil treatment,[13,14] fabric/textile repellency,[11,15] thermal management/latent heat transfer,[16,17] drag reduction,[18] structural insulation,[19] and fluidic devices.[20] These designed structures can be artificially constructed by various techniques like lithography,[10,21] templating/molding/imprinting,[22–24] plasma and chemical etching,[25,26] spin/dip/spray coating,[11,27,28] electrodeposition/electrospinning,[29] and chemical vapor deposition.[30,31] These methods often require intricate templates, complex multistep procedures, or a combination of several different methods that are highly process-intensive in order to achieve super-repellency. For example, many studies rely on photolithography to create the liquid repellent topological relief structures, a process that requires numerous steps, such as spin coating of a photoresist, ultraviolet light exposure through a photomask, and pattern development and etching. Further, many approaches rely on liquid-based processing that present challenges related to the use of solvents, including substrate damage, solvent residue, and poor coating quality.

The goal of achieving a superomniphobic coating or surface using a simple approach that overcome current processing challenges remain elusive. Here, we offer a one-step, direct and solvent-free approach for creating low surface energy textured surfaces with super liquid repellency by applying the initiated chemical vapor deposition (iCVD) process. iCVD vaporizes liquid precursors, typically monomers and initiators, to directly grow polymers on a variety of substrates. By bypassing the liquid phase, iCVD overcomes poor wettability and substrate damage often associated with liquid processing. The iCVD approach also provides precise process control and tunability to achieve desired polymer structure and properties without further post-treatment, such as removing solvent residues. The kinetics of iCVD polymerization reaction on the substrate surface is known to be controlled by monomer adsorption, i.e., the more monomer available at the surface the faster is the polymer growth. iCVD studies have shown that a simple parameter controls the overall deposition kinetics, which is the fractional saturation of monomer, z, defined as the ratio of the monomer partial pressure in the gas phase to its

Z. Chen, T. H. Nguyen, S. M. Rumrill, K. K. S. Lau
Department of Chemical and Biological Engineering
Drexel University
3141 Chestnut St, Philadelphia, PA 19104, USA
E-mail: klau@drexel.edu

The ORCID identification number(s) for the author(s) of this article can be found under https://doi.org/10.1002/admi.202101961.

DOI: 10.1002/admi.202101961

vapor pressure at the substrate surface ($z = P_M/P_{M,sat}$).[32,33] By controlling deposition kinetics, extremely conformal polymer coatings can be achieved, whereby the thickness of the coating is uniform across the topology of the underlying substrate. This property has been taken advantage of in order to create liquid repellent surfaces by iCVD previously. However, these attempts achieve super-liquid repellency by growing conformal fluoropolymer coatings onto textured templates, pre-roughened substrates, or intrinsically rough substrates, such as vertically aligned carbon nanotube forests,[34] electrospun fiber mats,[35] plasma-etched copper,[36] porous sponges,[37] fabrics,[38] and membranes.[39] It should be stressed that in these studies iCVD is only used to deposit conformal fluoropolymer coatings to lower the surface energy of the inherently rough substrate in order to create the necessary recipe for achieving super-liquid repellency. Common fluoropolymers used include poly(tetrafluoroethylene), and acrylate and methacrylate polymers with fluoroalkyl sidechains, such as poly(perfluorodecyl acrylate), poly(perfluorodecyl methacrylate), poly(perfluorooctyl methacrylate), and poly(hexafluorobutyl acrylate).

In general, it is much more difficult to achieve superoleophobicity compared to superhydrophobicity. Water, compared to organic oils, has a significantly higher liquid surface tension (72.89 mN m^{-1} for water vs 27.47 mN m^{-1} for hexadecane), which makes it easier for it to be dewetted and repelled from a low energy surface. Particularly, with a surface that has a roughly textured topology that is coated with a low surface energy fluoropolymer, water can achieve extremely high contact angles (>150°) as a result of being pinned by the rough surface structures that prevent it from imbibing and wetting the entire surface. This is known as the Cassie–Baxter state that describes a liquid droplet sitting on top of the textured surface with trapped air underneath.[6,7,40] In contrast, oil repellency, especially in air, is much more challenging to attain. Besides the need for a low energy surface, the textured surface must possess re-entrant structures, structures that have overhangs, caps, mushroom, umbrella, or convexly curved features, which create additional energy penalties against forming a wetting interface underneath.[10,41,42] Fabricating these re-entrant structures is technically challenging, although there are reports that intrinsically fibrous geometries, such as sponges and textiles, can yield superoleophobicity.[37,43,44] Here, in this work, we demonstrate iCVD as a liquid-free, one-step, bottom-up approach to fabricate a simultaneously superhydrophobic and superoleophobic (i.e., superomniphobic) surface on *flat, planar* substrates without the need to first create the textured surface topology or to use an intrinsically rough substrate. Specifically, we will show the deposition of a low surface energy polymer, poly(perfluorodecyl acrylate) (PPFDA), and the simultaneous formation of PPFDA worm-like structures (i.e., no longer a conformal thin coating) by simply tuning the iCVD process parameters. The iCVD process is believed to impact the evolution of crystallinity during the growth of semicrystalline PPFDA that then impacts the resulting polymer morphology. In this way, the processing scheme for enabling super-liquid repellency can be drastically simplified, reducing process intensity, eliminating liquid processing issues, and removing the need for additional substrate pre/post-treatments. This simplified process together with the use of planar substrates can make it easier to impart liquid repellency in current applications and potentially lead to a broader range of new application areas, such as in nanofluidics, nanoelectromechanical systems (NEMS), lab-on-a-chip devices, and nanorobotics, where controlled liquid repellency achievable without substrate templating or damage would be beneficial.

2. Results and Discussion

2.1. Deviation from Conformal Film Growth and the Appearance of Worm Structures

In iCVD, a polymer grows on a substrate surface by the free radical polymerization of monomer species. The monomer adsorbs from the vapor phase onto a substrate surface, where its polymerization is initiated by free radicals. The radicals form from gas phase peroxide initiator molecules that thermally dissociate over heated filament wires. To promote monomer adsorption, the substrate is typically kept at around room temperature. This is illustrated in **Figure 1** for the synthesis of PPFDA from perfluorodecyl acrylate (PFDA) monomer and di-*tert*-butyl peroxide (TBPO) initiator. Similar to other CVD techniques, iCVD yields highly conformal thin films on various substrates.[45] Particularly on flat planar substrates, like silicon wafers, iCVD can easily grow uniformly thin and contiguous coatings. Conformal coatings are particularly favored when the sticking probability of reactive species is low, and this usually occurs at higher substrate temperatures where adsorption is discouraged and the fractional saturation of monomer (z) is lower.[46] As shown in Figure 1, at a relatively high substrate temperature of 37 °C, we observe a relatively dense and contiguous film of PPFDA that is in line with iCVD PPFDA films reported previously.[47,48] Apart from small grain-like features, the film is contiguous and conforms to the underlying substrate topology, which in this case for the silicon wafer is flat and smooth. However, unexpectedly, by raising the substrate temperature further, we instead observe the PPFDA starting to deviate from conformal film growth, with large floret-like surface features forming at 42 °C, and then a more drastic shift to worm-like structures appearing at 46 °C. These worms appear to be randomly oriented as they protrude out from the surface. Remarkably, by increasing the substrate temperature to 48 °C, the surface morphology becomes smoother again with only some surface wrinkles, but any rough features of florets or worms have completely vanished. In contrast to the different physical morphologies observed by scanning electron microscopy (SEM), analysis of the deposited PPFDA by X-ray photoelectron spectroscopy (XPS) shows that the contiguous film and discrete worm-like structures have the same chemical composition as that expected of the PPFDA chemical structure, see Figure S0 (Supporting Information). This suggests that physical factors in the iCVD deposition of PPFDA and physical differences of the deposited PPFDA are what most likely contribute to the different morphologies shown in Figure 1 (see also Figure S1 for more detailed SEM visuals, Supporting Information).

These results illustrate that by simply adjusting the substrate temperature during the iCVD polymerization of PPFDA, PPFDA morphology can be dramatically changed, and the

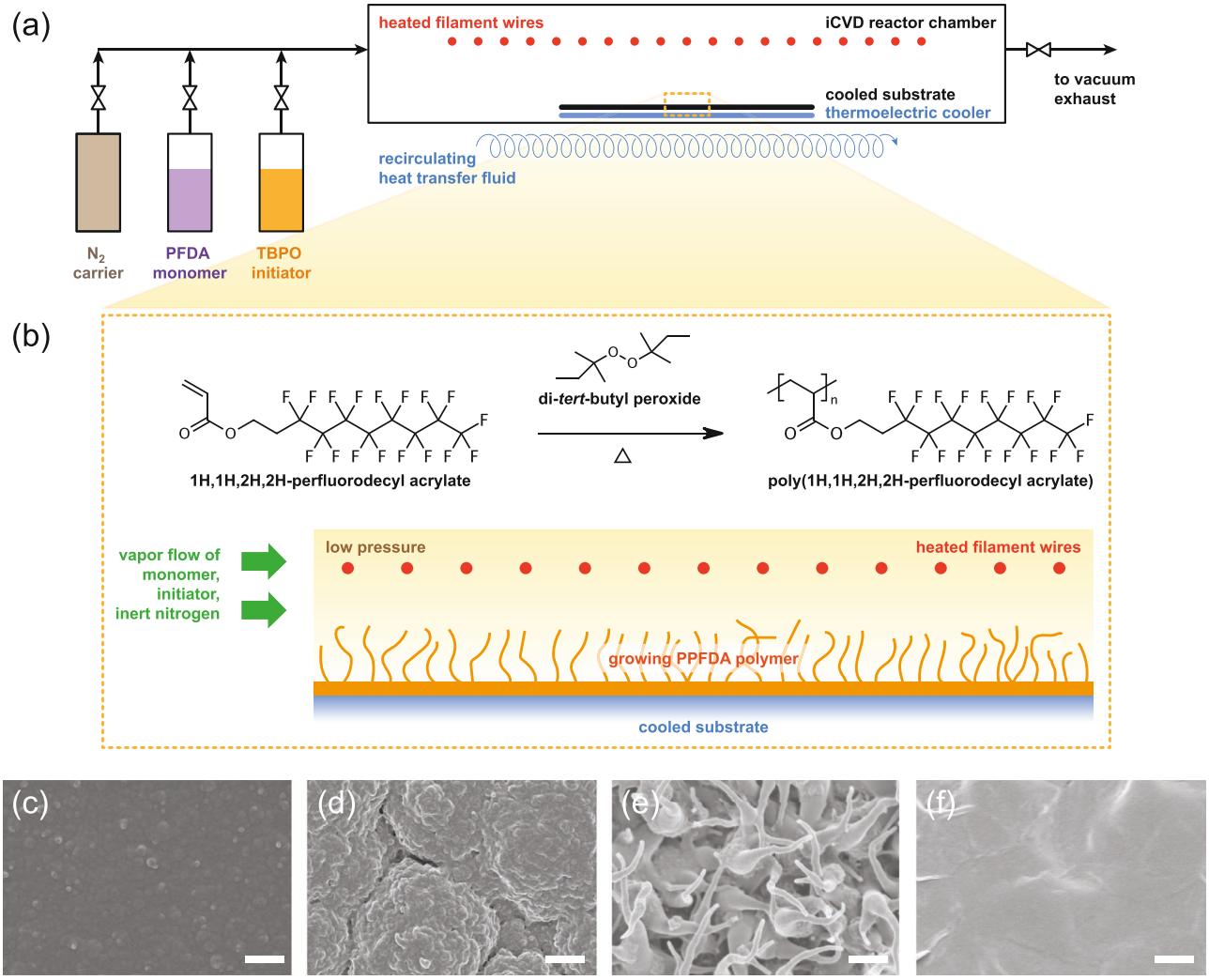

Figure 1. iCVD synthesis of PPFDA. a) iCVD reactor setup, and b) iCVD reaction scheme for the polymerization and growth of PPFDA. SEM top-down images of iCVD PPFDA grown at a substrate temperature of c) 37, d) 42, e) 46, and f) 48 °C. Scale bar is 1 µm.

appearance of the extremely rough, hierarchical worm-like structures of a low surface energy PPFDA fluoropolymer strongly suggests that the conditions are there to achieve high liquid repellency. Therefore, our goal in this report is to understand the role of the iCVD process in directing the growth of the worm features, which then impact liquid wetting behavior. This in turn helps us elucidate a possible mechanism for the development of worms as opposed to conformal film growth. Specifically, we investigated the effect of reactor pressure, inert (nitrogen) gas flow, substrate temperature, and deposition time, experimental details of which are described in the "Experimental Section" and summarized in **Table 1**. Previous literature reports on iCVD PPFDA have investigated the effect of iCVD processing parameters on PPFDA polymer chain crystallinity and crystalline structure,[47–49] but to our knowledge no studies have found extended worm-like structures that yield extreme liquid repellency, particularly to oils. Previous studies also did not achieve high liquid repellency on flat surfaces without prior substrate pretreatment or roughening. We should stress that in all of our studies here, PPFDA is grown directly

Table 1. Series of iCVD deposition studies and their respective process conditions.

Deposition series	Initiator flow rate [sccm]	Monomer flow rate [sccm]	Reactor pressure [mtorr]	N_2 inert flow rate [sccm]	Substrate temperature [°C]	Reaction time [min]
Reactor Pressure	0.20	0.12	90–190	0	46	45
Nitrogen Inert Flow Rate	0.20	0.12	90	0.10–0.50	46	45
Substrate Temperature	0.20	0.12	90	0.35	36–48	30
Reaction Time	0.20	0.12	90	0.35	46	3–120

on as-received flat, planar substrates, predominantly on smooth silicon wafers, without subjecting them to any surface pretreatment, templating, patterning, etching, roughening, etc., i.e., there are no steps made to artificially enhance the substrate surface roughness beforehand. We should also make it clear that, in presenting each deposition series that probe a specific iCVD process parameter, our discussions will first focus on understanding how a change in each process variable lead to a change in worm development and thereby change liquid wettability. These insights will then help us decipher the underlying mechanism by which worms can form, which then ultimately guide us in growing worms more generally on various substrate surfaces, again without any prior surface pretreatment to intentionally roughen the surface to achieve high liquid repellency.

2.2. Effect of Pressure

In iCVD, a higher reaction pressure generally leads to faster deposition and polymer growth as a result of a greater amount of monomer in the gas phase that promotes greater monomer adsorption on the substrate. To understand the influence of reactor pressure on worm growth, iCVD depositions were carried out at various pressures between 90 and 190 mtorr, while keeping a constant substrate temperature of 46 °C that yielded worms in our initial study (Table 1). The resulting PPFDA surface morphology, and the corresponding liquid wettability of water and hexadecane were probed, and the results are shown in **Figure 2** (see also Figure S2 for more detailed SEM visuals, Supporting Information). At all the pressures probed, we observe a noticeable dense layer of PPFDA film covering the silicon substrate (see cross-sectional SEM images), and also worm-like protrusions that change in their morphology with reactor pressure. At the highest pressure of 190 mtorr (pressure used in our initial study above), the worm features are highly tapered with a thick microscale base that narrows down to nanoscale tips, and the worms are randomly oriented and curling over (Figures 2a,b). When pressure is lowered to 140 mtorr, the worms become much thinner with a narrower base, and the worms show less tapering and curling (Figure 2c,d). At the lowest pressure of 90 mtorr, the worms are the narrowest with a much more uniform diameter from the base to the tip, and the worms are straighter, orienting predominantly in the vertical direction perpendicular to the silicon substrate plane (Figure 2e,f). These differences in surface morphologies translate directly to differences in the wetting behavior of liquid water and hexadecane droplets. As pressure decreases from 190 to 90 mtorr, the water contact angle decreases from 159° to 137°, while hexadecane contact angle decreases from 134° to 118° (Figure 2g). In all cases, the surfaces are hydrophobic and oleophobic (>90°), while the surface at the highest pressure of 190 mtorr is superhydrophobic (>150°).

Here, we can attempt to surmise the changes in surface morphology with reactor pressure, which then impacts liquid repellency. The more randomly oriented worms at higher pressures suggest a more uncontrolled and chaotic growth that could be due to the larger amount of monomer, which could promote more stochastic polymer nucleation and growth. In addition, the more significant sidewall tapering at higher pressures indicate polymer growth rate varies appreciably along the length of the worms as they grow. It is conceivable that, in addition to axial (vertical) growth by monomer adsorption at the worm tips, there is more radial (lateral) growth, particularly at the substrate surface, which is the cooler spot during iCVD and therefore where significantly more monomer would adsorb at the higher pressures. The rough worm-like surfaces coupled with PPFDA being one of the lowest surface energy polymers (around 120° water contact angle for a relatively smooth PPFDA film[50]) leads to the observed high liquid repellency. The greater repellency at higher pressures is most likely due to a general

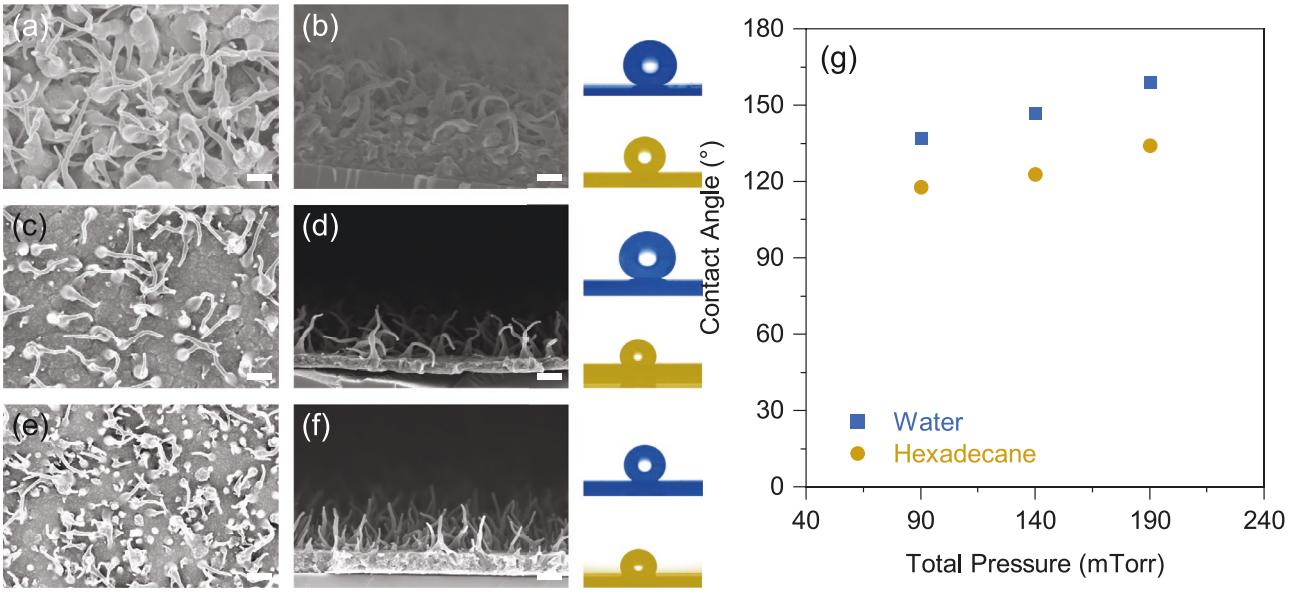

Figure 2. Effect of reactor pressure. SEM top-down and cross-sectional (left, right) images of iCVD PPFDA grown at a total pressure of a,b) 190, c,d) 140, and e,f) 90 mtorr. Scale bar is 1 µm. Corresponding water (blue) and hexadecane (yellow) droplet images (artificially colored), and g) their contact angles as a function of total pressure.

increase in surface roughness as the worms become more randomly oriented. There appears to be also more worms that are longer and curling over with higher pressure that further helps to create air pockets and discourage liquids from imbibing and wetting the surface.[41]

2.3. Effect of Inert Gas

Typically, nitrogen gas flow is introduced in iCVD as a way to systematically control monomer concentration and reaction kinetics.[51,52] The inert nitrogen gas molecules compete with the monomer for surface adsorption sites that can impede surface nucleation and growth of the polymer. To understand the influence of nitrogen inert, iCVD depositions were carried out at various nitrogen gas flow rates between 0.1 and 0.5 sccm, while keeping a constant substrate temperature of 46 °C and reactor pressure of 90 mtorr (Table 1). Although using 90 mtorr in our pressure study above did not yield the highest liquid repellency, it did provide the best control over worm growth and orientation due to the slower reaction kinetics, so we chose this pressure and added nitrogen here to intentionally slow down further the polymer growth rate. The resulting PPFDA surface morphology, and the corresponding liquid wettability of water and hexadecane are shown in **Figure 3** (see also Figure S3 for more detailed SEM visuals, Supporting Information). By adding a small amount of nitrogen flow at 0.10 sccm, the worms are fairly long (few µm), more randomly oriented, and rather tapered with large bases that extend to extremely fine tips (Figure 3a,b). By increasing the nitrogen flow to 0.35 sccm, we observe the worms now become shorter, straighter, and less tapered (Figure 3c,d). This trend continues as nitrogen flow increases to 0.50 sccm (Figure 3e,f). We further see that the spatial density of the worms and the thickness of the dense base layer decreasing when more nitrogen is added. Again, these surface morphology changes directly impact the observed liquid wetting behavior (Figure 3g). The lowest nitrogen flow of 0.10 sccm yields the most repellent surface with a water contact angle of ≈180° (to the point where it was not possible to capture a stable stationary droplet for measurement) and a hexadecane contact angle of 144°. This means the surface is superhydrophobic and near superoleophobic (>150°). By increasing the nitrogen flow to 0.35 sccm, the contact angles of water and hexadecane are slightly lower but still relatively high at 169° and 138°, respectively. At the highest nitrogen flow of 0.50 sccm, there is a sharp drop in contact angles of water and hexadecane to 133° and 90°, respectively.

The evolution of surface morphology with nitrogen flow and the impact on surface wettability generally matches the trend in the pressure study. The addition of nitrogen diluent, similar to the decrease in pressure, slows down growth kinetics that leads to more controlled worm growth with worms that are less tapered and more vertically oriented. This in turn translates to less surface roughness and fewer overhanging or re-entrant-type structures that deter liquid spreading. However, somewhat unexpected is the appearance of highly tapered and randomly oriented worms with a small addition of 0.10 sccm of nitrogen flow (Figure 3a,b). By slowing down the kinetics, we anticipated that the worms should grow more vertically and with even less tapering than the case without nitrogen, given all other deposition conditions were the same (compare with Figure 2e,f). To rationalize this seeming contradiction, we have to look at the change in the amount of PPFDA that grows as a dense base layer. Comparing the two cases, we see that this base layer is much thinner when 0.10 sccm of nitrogen is added, even though the worms are more disorganized and tapered. This leads us to hypothesize that the initial role of the nitrogen is to compete with monomer adsorption at the substrate surface that

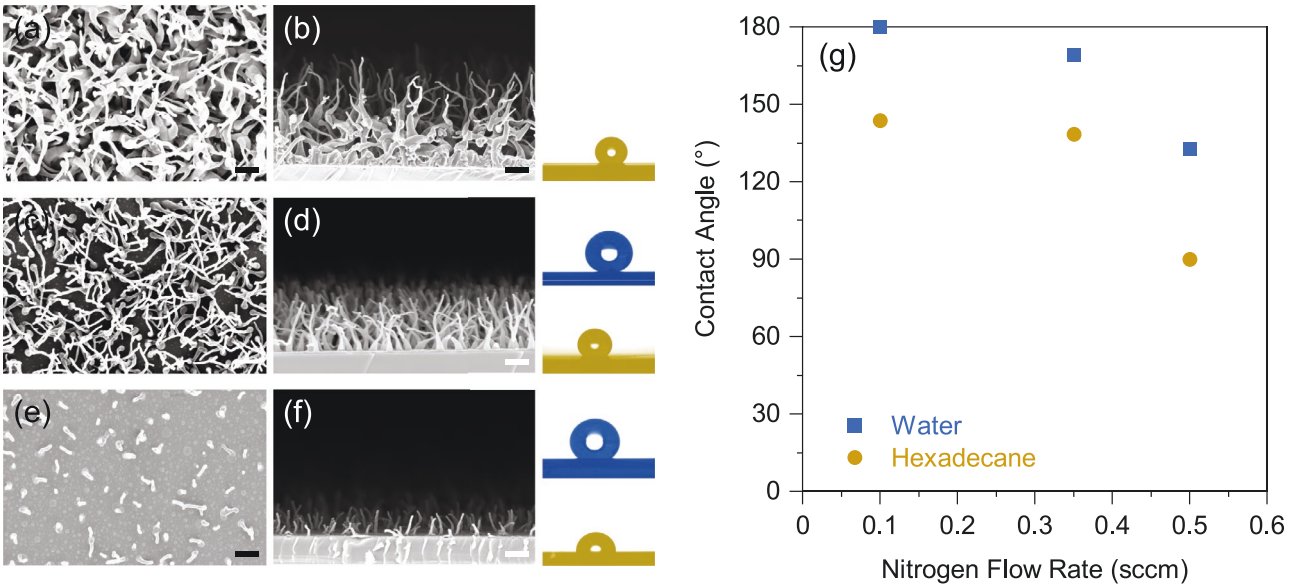

Figure 3. Effect of nitrogen inert. SEM top-down and cross-sectional (left, right) images of iCVD PPFDA grown at a nitrogen flow rate of a,b) 0.10, c,d) 0.35, and e,f) 0.50 sccm. Scale bar is 1 µm. Corresponding water (blue) and hexadecane (yellow) droplet images (artificially colored), and g) contact angles as a function of nitrogen flow rate (at 0.10 sccm, the water droplet did not remain stable enough on the surface to measure a static contact angle, so an angle of ≈180° has been assigned).

deters the growth of the dense base layer,[53] which then leads to a greater local monomer concentration available for enhancing lateral growth and tapering at the worm base. This is analogous to the high pressure effect seen in the previous pressure study. As more nitrogen is added, we believe there is a shift in its role to more of a diluting agent, where the presence of much more nitrogen now impacts the overall gas phase monomer concentration, slowing down overall kinetics and resulting in worms that are shorter, narrower, less tapered, more ordered and more vertical. At the highest nitrogen flow of 0.50 sccm, the dilution effect is so large that there are far fewer number of worms and the worms are much shorter, to the point that liquid repellency deteriorates significantly.

2.4. Effect of Substrate Temperature

Our initial study in Figure 1 demonstrates that substrate temperature is an important factor in influencing worm development. Here, we want to revisit the dependence on substrate temperature in the presence of nitrogen inert. We chose the intermediate flow of 0.35 sccm from the nitrogen inert study as a good balance between control of worm growth and liquid repellency. iCVD depositions were carried out at various substrate temperatures between 36 and 48 °C (Table 1). The resulting PPFDA surface morphology, and the corresponding liquid wettability of water and hexadecane are shown in **Figure 4** (see also Figure S4 for more detailed SEM visuals, Supporting Information). Unlike our initial study in Figure 1, where worms are seen only at 46 °C, the substrate temperature study here produced worm-like features at all substrate temperatures probed from 36 to 48 °C. Our initial study was carried out at a high pressure of 190 mtorr and without nitrogen, while the study here was made at 90 mtorr and with 0.35 sccm nitrogen. The lower pressure and nitrogen diluent slow down polymer growth appreciably and thereby widen the process window over which worms can develop and grow. Although worms are observed at all temperatures, there are some differences in worm morphology. At the lowest temperature of 36 °C, the worms are more disoriented, tapered, and curled over (Figure 4a,b), although the curling and tip extensions are not as appreciable compared to the ones seen in the pressure and nitrogen studies. At a higher substrate temperature of 44 °C, the worms now become more organized and less tapered, and stand much straighter and taller (Figure 4c,d). As substrate temperature increases further to 46 °C, the worm organization remains similar although the worms are shorter (Figure 4e,f), and at the highest substrate temperature of 48 °C, the worms are even shorter and thinner (Figure 4g,h). Although surface morphology show noticeable changes, the corresponding liquid wettability differences are not as significant (Figure 4i). In all cases, the surfaces are superhydrophobic (>150°) with slightly higher water contact angles (near 180°) at the highest substrate temperatures. However, the surfaces are only oleophobic with hexadecane contact angles in the range of 116° to 138°, and there does not appear to be any definite trend.

The general effect of a rise in substrate temperature is to make the worms grow straighter, thinner, and shorter, which means less polymer is deposited with a hotter substrate. This

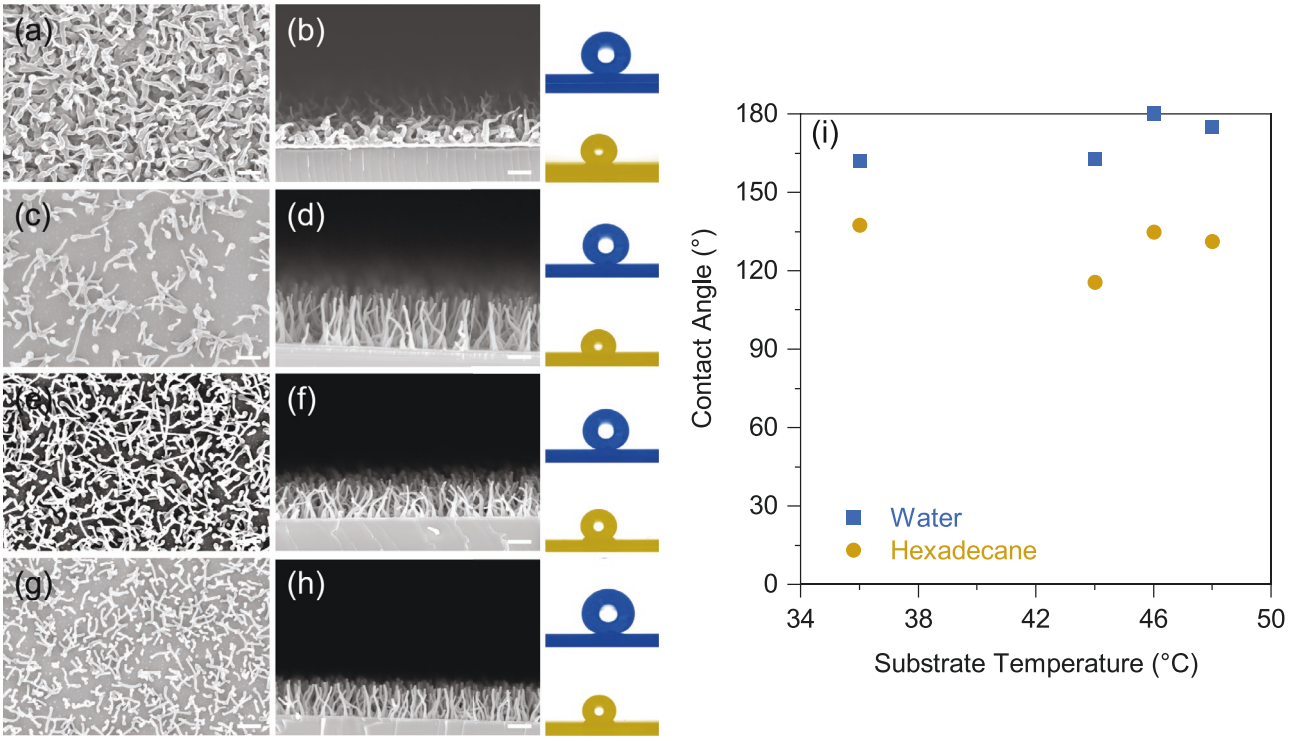

Figure 4. Effect of substrate temperature. SEM top-down and cross-sectional (left, right) images of iCVD PPFDA grown at a substrate temperature of a,b) 36, c,d) 44, e,f) 46, and g,h) 48 °C. Scale bar is 1 µm. Corresponding water (blue) and hexadecane (yellow) droplet images (artificially colored), and i) contact angles as a function of substrate temperature.

aligns with the slower deposition kinetics at higher substrate temperatures that is typical of the adsorption-limited iCVD polymerization process.[32,33] The worm tapering seen with the coldest substrate can be attributed to the greater monomer adsorption and surface concentration that favors more lateral and radial growth at the worm base, which is analogous to that seen in the pressure and nitrogen studies at their fastest worm growth conditions. Like these previous studies, we again see worms become more vertical, narrower, and less tapered as growth kinetics slow down. However, unlike these previous studies, the surface morphology changes with substrate temperature are relatively less drastic, which explains the smaller trends in liquid repellency. In all cases, the surface roughness is sufficient to impart superhydrophobicity. However, the absence of any significant re-entrant type structures, like overhangs, caps, or umbrella-type features that are required for strong oil repellency, means the surfaces do not attain superoleophobicity.

2.5. Effect of Reaction Time

The previous studies above have been carried out at a fixed reaction time. In this study, we want to follow worm evolution as a function of increasing reaction time from 3 to 120 min (Table 1). We chose a fixed condition (90 mtorr reactor pressure, 46 °C substrate temperature, and 0.35 sccm nitrogen inert flow) that represents a good balance between liquid repellency and worm organization based on studies above. The resulting PPFDA surface morphology, and the corresponding liquid wettability of water and hexadecane are shown in **Figure 5** (see also Figure S5 for more detailed atomic force microscopy (AFM) and SEM visuals, Supporting Information). At very short reaction times of 3 and 5 min, the surface is uniformly decorated with nanosized grains, roughly 200 nm in diameter (Figure 5a,b). At a longer deposition time of 7 min, the surface appears to be in the initial stages of worm development (Figure 5c,d). Discrete "heads" of the worms protrude from a very thin, dense, and uniform polymer layer, and they are spaced randomly on the surface. After 10 min, the worms are noticeably longer, with each worm at roughly the same height (Figure 5e,f). The worms are narrowly thin and without any noticeable tapering, but the number of worms is much less compared to the protrusions that appear at 7 min. Many of the initial protrusions seem to have been absorbed into the thickened dense base layer as evidenced by the many small bumps that can be seen on this surface. With even longer reaction times of 20 and 30 min, the general trend is the worms that "survive" continue to grow longer, while the dense base layer does not appear to thicken further, and so the total spatial density of the worms remains roughly unchanged (Figure 5g–j). However, at longer reaction times of 45 and 120 min, the worms become more disorganized (Figure 5k–n). The worms have more tapered bases and are significantly less vertically oriented, with curled over tips that point in random directions.

This surface morphology evolution is reflected in the corresponding changes in liquid repellency (Figure 5o). At short reaction times (3, 5, and 7 min), when worms are absent or barely formed, the low surface roughness yields low water and hexadecane contact angles that are close to the values for a relatively smooth and conformal iCVD PPFDA film coated on silicon, which we measure to be around 120° and 90°, respectively. As the worms become well-defined and grow taller (10, 20, and 30 min), the surface becomes rougher and more space is created between the worm tip and the worm base, where air pockets can form and act to keep liquids from spreading. This is apparent with liquid water on these surfaces as the water contact angles exceed 150°, indicating superhydrophobicity. However, at these times, the worms are fairly straight and uniformly tall. As a result, the surface lacks the re-entrant structures, i.e., structures that do not just point straight up, that superoleophobicity demands, and so hexadecane contact angles though increasing with reaction time are below 150°. At the longest reaction times (45 and 120 min), the surface roughness remains high and the surface remains superhydrophobic. Any variability or fluctuation in water contact angle above 150° as mentioned before is due to practical difficulties in maintaining a stable, static water droplet for angle measurements. With the appearance of curled up worms and more random worm orientations that create a mesh-like network and mimic re-entrant type features, the hexadecane contact angle approaches and reaches the superoleophobic limit, where at 120 min the oil contact angle is 155°.

2.6. Mechanism of Worm Formation

Our studies above have probed the influence of key iCVD reaction parameters on worm development and surface morphology that directly impacts liquid wettability and repellency. First, we see that, in all cases, slower reaction kinetics favor worms to appear and grow in a more orderly manner, regardless of whether kinetics are slowed down by decreasing reactor pressure, adding nitrogen inert, or increasing substrate temperature. All these changes lead to less monomer available for surface polymerization that limits polymerization kinetics. Second, we see that, in all cases, faster growth kinetics lead to more worm tapering. This tapering is attributed to significant lateral growth at the worm base compared to at the worm tip due to more monomer available locally at or near the surface that occurs with a higher reactor pressure, less nitrogen, or a cooler substrate. We therefore can conclude that surface polymerization kinetics has a significant impact on worm development. However, our studies so far have not addressed an important question. What drives iCVD PPFDA to form worms rather than a conformal thin film? In general, CVD processes, including iCVD, achieves highly conformal and uniform thin films easily, particularly on smooth, openly flat substrates like silicon wafers. Even on nonplanar substrates, such as trenches,[54] porous membranes/fibers/networks,[35,55,56] or tubular/wire arrays,[34,57] iCVD has shown that highly conformal coatings around complex surface topologies can be achieved by reducing the monomer sticking coefficient or reaction probability.[46,56] We have shown in our previous work that this can be done by lowering the fractional monomer saturation (z) at the surface, which then limits reaction kinetics relative to monomer diffusion.[32,33] Yet contrary to this, slower kinetics in our processing studies here seem to favor forming worms rather than a conformal thin film. This apparent contradiction suggests

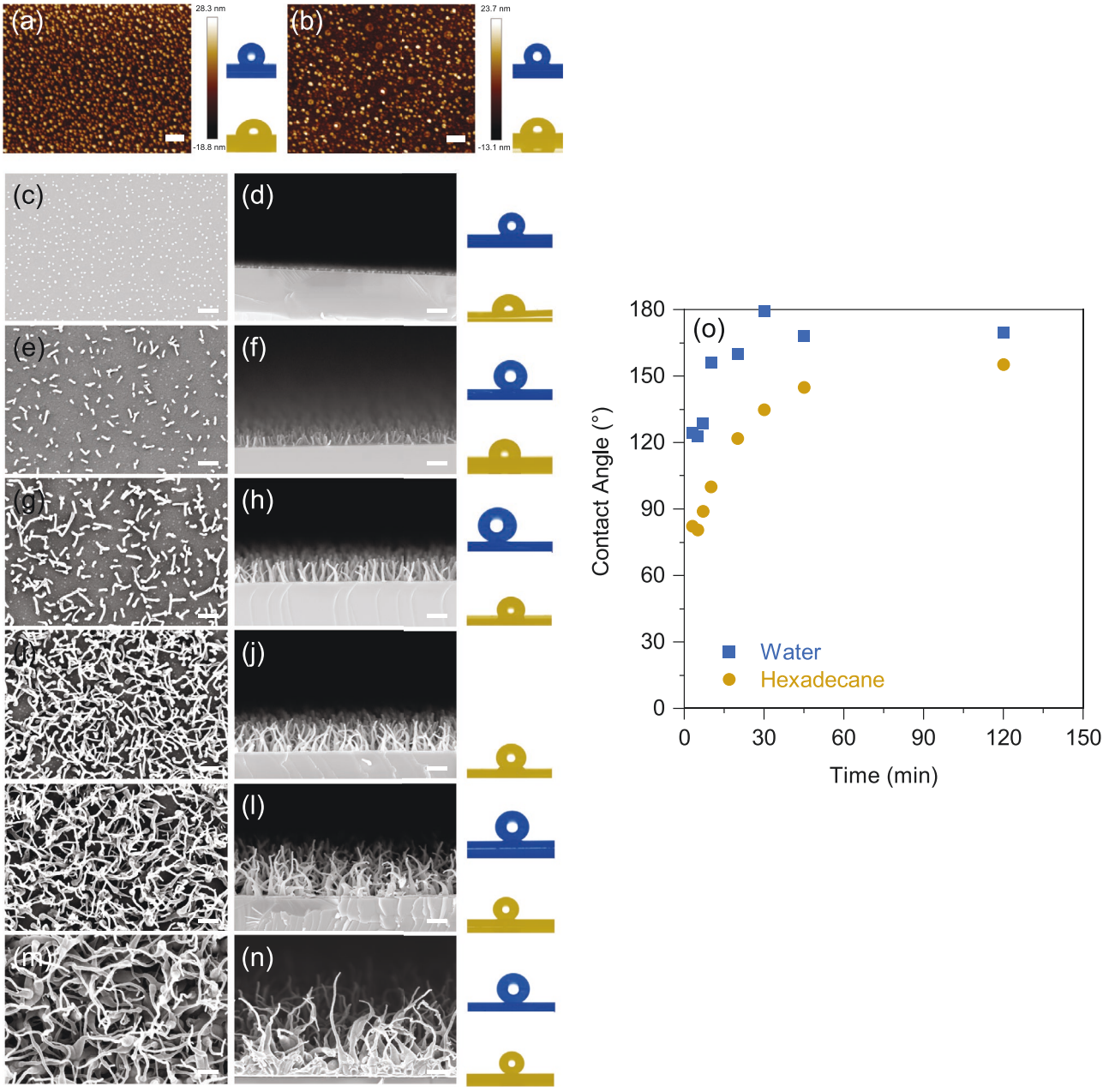

Figure 5. Effect of reaction time. AFM images of iCVD PPFDA grown for a) 3, and b) 5 min. SEM top-down and cross-sectional (left, right) images of iCVD PPFDA grown for c,d) 7, e,f) 10, g,h) 20, i,j) 30, k, l) 45, and m,n) 120 min. Scale bar is 1 µm. Corresponding water (blue) and hexadecane (yellow) droplet images (artificially colored), and o) contact angles as a function of reaction time.

that there could be a specific driving force present in the iCVD polymerization of PPFDA that induces worms to form, and for the polymer to spatially grow selectively and preferentially.

Here, we propose that the driving force and mechanism for preferential worm formation is related to the semicrystalline nature of PPFDA, see **Figure 6**. PPFDA has a repeat unit structure with a long C8 fluorocarbon pendant sidechain (Figure 1). We know from literature that these fluorinated sidechains easily self-assemble into a liquid crystalline state, mainly as a smectic B phase composed of bilayers of the pendant fluorinated groups that pack themselves into a hexagonal array within a lamellar structure (Figure 6a–c).[58–60] For iCVD PPFDA, this liquid crystalline structure has also been confirmed by prior X-ray diffraction (XRD) studies on conformal thin films.[47–49] Significantly, from literature, we see that monomers containing liquid crystalline sidechains, like C8 fluorocarbons and stilbene, can polymerize in the liquid phase into worms and nanowires.[61,62] Interestingly, these studies, which are examples of polymerization induced self-assembly (PISA) methods, find evidence that the sidechains orient themselves parallel to the worm or wire axis, i.e., the lamellar plane is perpendicular to the growth direction. For example, in the block copolymerization

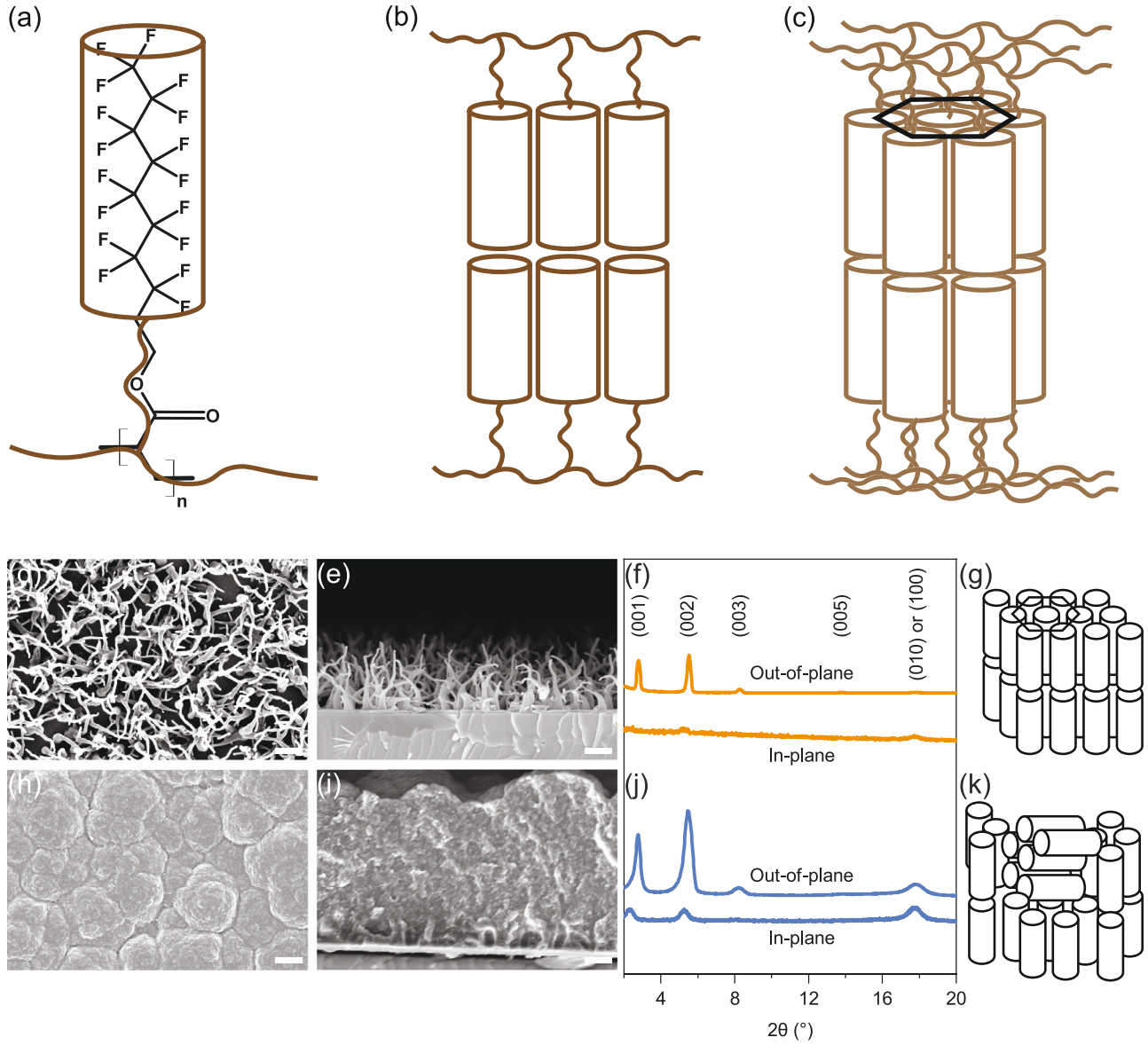

Figure 6. Crystalline arrangement of PPFDA. a) C8 fluorocarbon sidechain of each repeat unit of the PPFDA polymer pack together in b) a bilayer structure that extends into c) a hexagonal array and lamellar structure. d,e) SEM top-down and cross-sectional (left, right) images of iCVD PPFDA grown as discrete worm structures, f) corresponding out-of-plane and in-plane XRD data, and g) proposed PPFDA sidechain and lamellar arrangement perpendicular and parallel to the silicon substrate, respectively. h,i) SEM top-down and cross-sectional (left, right) images of iCVD PPFDA grown as a contiguous film with floret structures, j) corresponding out-of-plane and in-plane XRD data, and k) proposed PPFDA sidechain and lamellar arrangement that is randomly distributed. SEM scale bar is 1 µm.

of a series of methacrylate monomers containing different fluorinated sidechain lengths (C4, C6, and C8) with a macroinitiator in solution, self-assembled worm-like morphologies form most favorably with the longest fluorinated sidechain, i.e., with perfluorodecyl methacrylate, which is the methacrylate version of the acrylate monomer we used here.[63] The cylindrical worm formation is attributed to strong liquid crystalline ordering of the C8 fluorocarbon sidechains that stacks the growing polymer chains in layers as the worm builds up. We should note though that these PISA studies have been done in a solvent phase. In a chemical vapor deposition environment, literature shows nanowires, nanofibers, and nanopillars have also been grown predominantly with crystalline materials, such as silicon, germanium, and carbon.[64,65] Although the growth of such 1D nanostructures is generally defined and aided by catalyst seed particles, their crystallinity is one primary factor that dictates the growth front, which is primarily in the direction in which the growth plane has the lowest surface energy.[66] For example, silicon, germanium, and diamond nanowires are known to grow along the (111) direction where the lowest energy (111) crystal plane interfaces with the catalyst surface at the growth front.[66,67] It is therefore likely that the growth of polymer nanowires with liquid crystalline sidechains could also be driven by minimizing surface energy. The C8 fluorocarbon sidechains, in

particular with their CF_3 ends groups that are among the lowest surface energy chemical groups, would favor a CF_3-rich growth plane that orients the sidechains parallel to the growth axis.

Thus, we hypothesize that liquid crystalline ordering of C8 fluorocarbon sidechains during iCVD synthesis drives PPFDA worm nucleation and growth. To test this hypothesis, we performed in-plane and out-of-plane XRD measurements to elucidate the crystalline nature of PPFDA worm structures grown with slower kinetics at 46°C substrate temperature, 90 mtorr reactor pressure, and with 0.35 sccm of nitrogen flow (Figure 6d–g), and compare it to that of a PPFDA film containing no worms grown with faster kinetics at 42 °C substrate temperature, 190 mtorr reactor pressure, and without any nitrogen flow (Figure 6h–k) (see also Figure S6 for more detailed SEM visuals, Supporting Information). For PPFDA worms, the out-of-plane XRD data shows strong (001) and (002) peaks as well as weaker higher order (003) and (005) peaks, and the near absence of the (010) or (100) peak. In contrast, the in-plane XRD data of the worms shows that the (001) and its higher order peaks nearly vanish, and instead the (010) or (100) peak appears to be dominant. Since the (001) and its higher order peaks are associated with the fluorinated sidechain bilayer structure,[58–60] the disappearance of these peaks in the substrate plane strongly indicate that these bilayer structures are oriented perpendicular to the silicon plane, or equivalently the lamellar plane is perpendicular to the worm's growth axis (Figure 6g). This agrees with observations of liquid crystalline alignment in polymer nanowires grown in the liquid phase by PISA in which the liquid crystalline sidechain axis is parallel to the worm axis. It also aligns with the observations that the growth plane of nanowires grown by CVD is generally of the lowest surface energy, which for PPFDA is the CF_3-rich lamellar plane, since fluorocarbons, like CF_3 and CF_2, are known to be some of the lowest surface energy moieties (CF_3: 6 mN m^{-1}; CF_2: 18 mN m^{-1};), while hydrocarbons, like CH_3, CH_2, and = CH, are higher (CH_3: 22 mN m^{-1}; CH_2: 31 mN m^{-1}; = CH: 33 mN m^{-1}).[68] In contrast, for the PPFDA film without worms, all the XRD peaks associated with crystalline PPFDA are observed in both out-of-plane and in-plane XRD data. This means that the liquid crystalline structures are more randomly oriented on the silicon substrate without any preferential growth direction that would promote worm development (Figure 6k).

Based on the crystallization-directed worm growth mechanism, we can postulate that the change from a film to worm morphology with slower polymerization kinetics could be due to a competition between polymer chain propagation (addition of monomer units to a growing chain) and polymer chain crystallization (orientation of monomer units in a growing chain). Under slow reaction conditions, we believe there is sufficient time for monomer molecules to orient themselves with their sidechains packing vertically before their configurations are locked in by the polymerization reaction. In contrast, under fast reaction conditions, the monomer is consumed by polymerization very quickly, making it hard for the monomer to orient favorably, leading to kinetically trapped orientations that are more randomly directed. Based on our proposed mechanism, we can also consider the process by which the worms might evolve over time (Figure 5). At very short times, there is not enough PPFDA to assemble into sizeable worms but the presence of small PPFDA particles already indicates worm nucleation and growth has already started. As time progresses and more PPFDA forms, the worms start to grow out more but their growth is impacted by the simultaneous growth of the dense base layer. This base layer most likely consists of more randomly oriented liquid crystalline domains unlike in the worms where the liquid crystalline sidechains are vertically arranged into the lowest energy growth plane. Initially, base layer growth seems to dominate since many of the worm protrusions disappear into this growing film. Later on, the worms seem to grow more preferentially as the worms that survive continue to grow out longer while the base layer growth seems to be arrested. This suggests that, as the worms grow, more monomer preferentially adsorbs and polymerizes on the worms' growth plane rather than at the base layer surface due to the favorable crystallization-driven process. At much longer times, the worms, which start out orienting mostly upwards as they grow, now begin to curl significantly. This curling could be related to defects in the liquid crystalline order since the probability of defects would increase with increasing reaction time. There is very similar evidence from PISA that shows liquid crystalline cylinders starting to bend as the degree of polymerization of the fluorinated block increases.[69] This bending has been attributed to a mismatch in the liquid crystalline planes that are tolerated even as the cylinders grow longer.[70]

2.7. Worm Growth Potential

Our studies above have focused on growing worms on bare silicon wafers. To demonstrate a broader potential, depositions were additionally made on a variety of other substrates, including planar and nonplanar ones. **Figure 7** shows examples of worms grown on planar copper and chromium metal surfaces that were thermally evaporated (20 nm metal film) over silicon wafer substrates as well as on a nonplanar stainless steel mesh (400 × 400 mesh) (see also Figure S7 for more detailed SEM visuals, Supporting Information). The ability to grow worms regardless of the substrate material or topology indicates that the underlying substrate has less of an impact on the development of PPFDA crystallinity and worm growth. Instead, our work highlights the importance of iCVD processing in controlling polymerization kinetics and crystalline alignment for worm development.

3. Conclusion

To date, direct growth of polymer micro- and nanostructures has not been clearly demonstrated by iCVD or other polymer CVD methods, such as plasma polymerization, vapor deposition polymerization, and molecular deposition. In addition, current approaches, whether solvent-free or solvent-based, have largely relied on various surface pretreatment strategies like lithography, patterning, templating, etching, and roughening to create surface roughness, texture, and re-entrant structures to achieve superhydrophobicity and superoleophobicity. Here, our iCVD work achieves superomniphobicity by constructing micro- and nanoworms of a liquid crystalline fluorinated

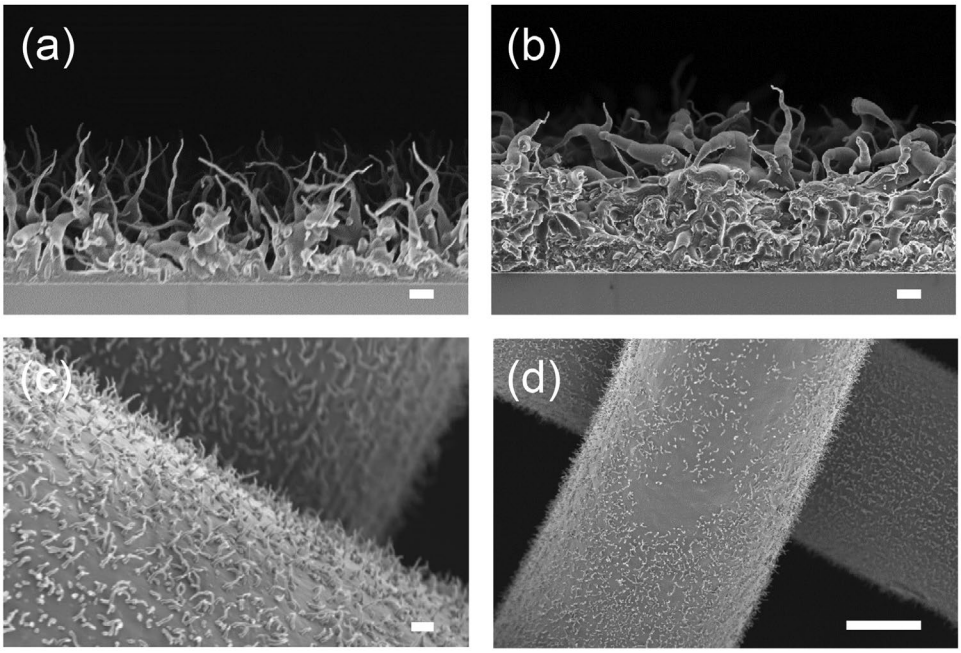

Figure 7. Worm growth on different substrates. SEM cross-sectional images of iCVD PPFDA grown on a) copper, and b) chromium surface, thermally evaporated as a 20 nm film on a silicon substrate. SEM top-down images of iCVD PPFDA grown on c,d) 400 × 400 stainless steel wire mesh. Scale bars are 1 µm a–c) and 10 µm d).

polymer directly on planar substrates without requiring surface pretreatment. Worm are favored over a contiguous thin film due to crystallization-directed nucleation and growth that is much like the emerging polymerization induced self-assembly (PISA) process carried out in the solvent phase, except iCVD does not use any solvent nor block copolymerization to drive phase separation and crystalline alignment. The ability to directly create highly liquid repelling, superomniphobic surfaces over a wide range of substrates without special substrate treatment or liquid processing is anticipated to enable micro- and nanoscale applications in fluidics, miniature reactors, and separators, electromechanical systems, lab-on-a-chip devices, and robotics.

4. Experimental Section

Substrate Preparation: Primarily, substrates were silicon wafers (PureWafer) and used as-received. In addition, copper and chromium-coated silicon substrates were used, and prepared by evaporating 20 nm thin films using a thermal evaporator (VE90, Thermonics) with copper and chromium targets (Kurt J. Lesker). Stainless steel wire mesh (400 × 400 mesh, McMaster-Carr) was also used as a substrate, and was cleaned of surface contaminants by an ethanol rinse, followed by nitrogen drying and then an air plasma (Harrick Plasma). The uncoated and coated silicon wafers were cut to a size of 40 × 40 mm^2, while the stainless steel mesh was cut to a size of 80 × 40 mm^2.

iCVD Reactor Setup: The iCVD reactor is a custom-built stainless steel reactor, 21 × 21 × 4 cm^3 in internal volume, with a 2.5 cm thick quartz window as the reactor lid. The substrate was placed on a temperature-controlled thermoelectric cooler (TEC, 40 × 40 mm^2, Custom Thermoelectric), which was attached to the temperature-controlled reactor stage using vacuum-stable thermal grease (Heat-Away 641-EV, Aremco Products) that ensured good thermal contact between the TEC and reactor stage. The reactor stage temperature was controlled through backside contact with a silicone oil flowing through a recirculating chiller (Neslab RTE7, Thermo Scientific) set to a temperature of 50 °C. The TEC was connected to a DC power supply (6623A, Agilent), which was set to a constant voltage of 10.0 V. A solid-state relay (Omega Engineering), acting as an on/off switch in the TEC power circuit, and connected with a temperature controller (Omega Engineering) and a K-type thermocouple attached to the top surface of the substrate, was used to control the substrate temperature. A HeNe laser (JDS Uniphase) together with a silicon photodetector (Gentec-EO) was used to monitor the in situ growth of the polymer on the substrate by laser interferometry. A set of 12 Chromaloy filament wires (0.5 mm diameter, Goodfellow) was placed 1.6 cm above the substrate, and resistively heated to ≈270 °C using a DC power supply (Vol Teq) set to a constant voltage of 19 V (1.1 A). A rotary vacuum pump (E2M30, Edwards), a Baratron capacitance manometer (626C, MKS Instruments), and a downstream throttle valve (153D, MKS Instruments) were used to automatically maintain a set pressure inside the reactor chamber.

iCVD Synthesis: Di-*tert*-butyl peroxide (TBPO, 99% Acros Organics) and 1H,1H,2H,2H-perfluorodecyl acrylate (PFDA, 99.6% Fluoryx) were used as the initiator and monomer, respectively, without further purification. The volatile initiator was kept at room temperature as it had sufficient head pressure without any heating. The TBPO initiator flow rate, set at 0.20 sccm (standard cubic centimeter per minute), was controlled by a precision needle valve (Swagelok). The PFDA monomer was heated to 80 °C to achieve enough head pressure, and using a separate precision needle valve (Swagelok), the monomer flow rate was maintained at 0.12 sccm. When used, nitrogen inert gas (Airgas) was delivered through an automated mass flow controller (1479A, MKS Instruments). The initiator, monomer, and nitrogen vapor flows were delivered to the reactor via heated 0.25 in. diameter stainless steel tubing. As shown in Table 1, four separate iCVD deposition series were performed to determine separately the effect of reactor pressure, nitrogen inert flow, substrate temperature, and reaction time on PPFDA polymer growth. For each series, only the process variable of interest was varied while all other reaction conditions were kept constant.

Characterization: SEM was primarily used to physically characterize surface morphology. To minimize surface charging of the insulating

polymer, the samples were coated with Pt/Pd using a sputter coater (Cressington 208 HR) at 40 mA for 30 s. To ensure even coating, the samples were positioned in the sputter coater at angle of 45° and continuously rotated. Top-down and cross-sectional SEM were performed on a Zeiss Supra 50VP with an accelerating voltage at 2–4 kV and a working distance at ~5 mm. AFM was also performed on the samples, with images captured in air by tapping mode on a Bruker Dimension Icon with an Al-coated cantilever tip (HQ:NSC15/Al BS, Mikromasch) and data processed with NanoScope Analysis software. X-ray photoelectron spectroscopy (XPS) was used to elucidate chemically the deposited polymer composition. XPS was conducted on a Physical Electronics PHI 5000 VersaProbe using monochromatic Al Kα (1486.6 eV) excitation at 25 W with charge compensation on the insulating samples. High-resolution C1s scans were acquired from 280 to 302 eV with a pass energy of 23.5 eV. The wettability of the substrate surfaces was characterized by measuring the contact angle of droplets of different probe liquids on the surface. Stationary droplets of 3–14 µL of deionized water and 3 µL of hexadecane (99%, Alfa Aesar) were separately deposited on the surface in air. Water and hexadecane were chosen as test liquids with different surface tensions (water: 72.89 mN/m; hexadecane: 27.47 mN/m at 20 °C) to evaluate water and oil repellency. Contact angles were measured on an automated contact angle goniometer (Model 290, ramé-hart instrument) and data was processed by DROPimage Advanced software.

Supporting Information

Supporting Information is available from the Wiley Online Library or from the author.

Acknowledgements

The work was supported by the U.S. National Science Foundation (CBET-1510888 and CMMI-1950964) and the U.S. Department of Education under the Graduate Assistance in Areas of National Need fellowship program (GAANN Award No. P200A190027). The authors also acknowledge the use of facilities in the Materials Characterization Core at Drexel University and in the Singh Center for Nanotechnology at the University of Pennsylvania, which is supported by the NSF National Nanotechnology Coordinated Infrastructure Program (NNCI-2025608).

Conflict of Interest

The authors declare no conflict of interest.

Data Availability Statement

The data that support the findings of this study are available from the corresponding author upon reasonable request.

Keywords

initiated chemical vapor deposition (iCVD), nano/microworms, semicrystalline fluoropolymer, superhydrophobicity, superoleophobicity

Received: October 10, 2021
Revised: January 23, 2022
Published online:

[1] V. Zorba, E. Stratakis, M. Barberoglou, E. Spanakis, P. Tzanetakis, S. H. Anastasiadis, C. Fotakis, *Adv. Mater.* **2008**, *20*, 4049.
[2] J. Yong, F. Chen, Q. Yang, J. Huo, X. Hou, *Chem. Soc. Rev.* **2017**, *46*, 4168.
[3] R. Hensel, A. Finn, R. Helbig, H. Braun, C. Neinhuis, W. Fischer, C. Werner, *Adv. Mater.* **2014**, *26*, 2029.
[4] H. Bellanger, T. Darmanin, E. T. de Givenchy, F. Guittard, *Chem. Rev.* **2014**, *114*, 2694.
[5] R. N. Wenzel, *Ind. Eng. Chem.* **1936**, *28*, 988.
[6] A. B. D. Cassie, *Discuss. Faraday Soc.* **1948**, *3*, 11.
[7] A. B. D. Cassie, S. Baxter, *Trans. Faraday Soc* **1944**, *40*, 546.
[8] W. Barthlott, C. Neinhuis, *Planta* **1997**, *202*, 1.
[9] S. Herminghaus, *Europhys. Lett.* **2000**, *52*, 165.
[10] A. Tuteja, W. Choi, M. Ma, J. M. Mabry, S. A. Mazzella, G. C. Rutledge, G. H. McKinley, R. E. Cohen, *Science* **2007**, *318*, 1618.
[11] S. Pan, R. Guo, M. Björnmalm, J. J. Richardson, L. Li, C. Peng, N. Bertleff-Zieschang, W. Xu, J. Jiang, F. Caruso, *Nat. Mater.* **2018**, *17*, 1040.
[12] Y. Lu, S. Sathasivam, J. Song, C. R. Crick, C. J. Carmalt, I. P. Parkin, *Science* **2015**, *347*, 1132.
[13] Z. Xu, Y. Zhao, H. Wang, X. Wang, T. Lin, *Angew. Chem., Int. Ed.* **2015**, *54*, 4527.
[14] X. Q. Cheng, Y. Jiao, Z. Sun, X. Yang, Z. Cheng, Q. Bai, Y. Zhang, K. Wang, L. Shao, *ACS Nano* **2021**, *15*, 3500.
[15] S. Pan, R. Guo, W. Xu, *AIChE J.* **2014**, *60*, 2752.
[16] I. U. Vakarelski, N. A. Patankar, J. O. Marston, D. Y. C. Chan, S. T. Thoroddsen, *Nature* **2012**, *489*, 274.
[17] B. Mondal, M. M. G. Eain, Q. Xu, V. M. Egan, J. Punch, A. M. Lyons, *ACS Appl. Mater. Interfaces* **2015**, *7*, 23575.
[18] K. N. Al-Milaji, H. Zhao, *Appl. Surf. Sci.* **2017**, *396*, 955.
[19] Z. Ma, X. Liu, X. Xu, L. Liu, B. Yu, C. Maluk, G. Huang, H. Wang, P. Song, *ACS Nano* **2021**, *15*, 11667.
[20] E. Gogolides, K. Ellinas, A. Tserepi, *Microelectron. Eng.* **2015**, *132*, 135.
[21] J.-Y. Shiu, C.-W. Kuo, P. Chen, C.-Y. Mou, *Chem. Mater.* **2004**, *16*, 561.
[22] X. Deng, L. Mammen, H.-J. Butt, D. Vollmer, *Science* **2012**, *335*, 67.
[23] B. Li, J. Zhang, Z. Gao, Q. Wei, *J. Mater. Chem. A* **2016**, *4*, 953.
[24] Y. Wu, J. Zeng, Y. Si, M. Chen, L. Wu, *ACS Nano* **2018**, *12*, 10338.
[25] D.-H. Ko, W. Ren, J.-O. Kim, J. Wang, H. Wang, S. Sharma, M. Faustini, D.-P. Kim, *ACS Nano* **2016**, *10*, 1156.
[26] J. Ryu, K. Kim, J. Park, B. G. Hwang, Y. Ko, H. Kim, J. Han, E. Seo, Y. Park, S. J. Lee, *Sci. Rep.* **2017**, *7*, 1981.
[27] D. Xiong, G. Liu, L. Hong, E. J. S. Duncan, *Chem. Mater.* **2011**, *23*, 4357.
[28] H. Wang, Y. Xue, J. Ding, L. Feng, X. Wang, T. Lin, *Angew. Chem., Int. Ed.* **2011**, *50*, 11433.
[29] V. A. Ganesh, S. S. Dinachali, H. K. Raut, T. M. Walsh, A. S. Nair, S. Ramakrishna, *RSC Adv.* **2013**, *3*, 3819.
[30] G. R. J. Artus, S. Jung, J. Zimmermann, H. -P. Gautschi, K. Marquardt, S. Seeger, *Adv. Mater.* **2006**, *18*, 2758.
[31] J. Zimmermann, M. Rabe, G. R. J. Artus, S. Seeger, *Soft Matter* **2008**, *4*, 450.
[32] K. K. S. Lau, K. K. Gleason, *Macromolecules* **2006**, *39*, 3688.
[33] K. K. S. Lau, K. K. Gleason, *Macromolecules* **2006**, *39*, 3695.
[34] K. K. S. Lau, J. Bico, K. B. K. Teo, M. Chhowalla, G. A. J. Amaratunga, W. I. Milne, G. H. McKinley, K. K. Gleason, *Nano Lett.* **2003**, *3*, 1701.
[35] M. L. Ma, Y. Mao, M. Gupta, K. K. Gleason, G. C. Rutledge, *Macromolecules* **2005**, *38*, 9742.
[36] I. Vilaró, J. L. Yagüe, S. Borrós, *ACS Appl. Mater. Interfaces* **2017**, *9*, 1057.
[37] D. Kim, H. Im, M. J. Kwak, E. Byun, S. G. Im, Y.-K. Choi, *Sci. Rep.* **2016**, *6*, 29993.
[38] D. Soto, A. Ugur, T. A. Farnham, K. K. Gleason, K. K. Varanasi, *Adv. Funct. Mater.* **2018**, *28*, 1707355.

[39] M. Gupta, V. Kapur, N. M. Pinkerton, K. K. Gleason, *Chem. Mater.* **2008**, *20*, 1646.
[40] S. Baxter, A. B. D. Cassie, *J. Text. Inst. Trans.* **1945**, *36*, T67.
[41] A. Tuteja, W. Choi, J. M. Mabry, G. H. McKinley, R. E. Cohen, *Proc. Natl. Acad. Sci. USA* **2008**, *105*, 18200.
[42] A. Tuteja, W. Choi, G. H. McKinley, R. E. Cohen, M. F. Rubner, *MRS Bull.* **2008**, *33*, 752.
[43] S. Michielsen, H. J. Lee, *Langmuir* **2007**, *23*, 6004.
[44] W. Choi, A. Tuteja, S. Chhatre, J. M. Mabry, R. E. Cohen, G. H. McKinley, *Adv. Mater.* **2009**, *21*, 2190.
[45] P. Moni, A. Al-Obeidi, K. K. Gleason, *Beilstein J. Nanotechnol.* **2017**, *8*, 723.
[46] S. H. Baxamusa, K. K. Gleason, *Chem. Vap. Deposition* **2008**, *14*, 313.
[47] A. M. Coclite, Y. Shi, K. K. Gleason, *Adv. Funct. Mater.* **2012**, *22*, 2167.
[48] A. M. Coclite, Y. Shi, K. K. Gleason, *Adv. Mater.* **2012**, *24*, 4534.
[49] A. Perrotta, P. Christian, A. O. F. Jones, F. Muralter, A. M. Coclite, *Macromolecules* **2018**, *51*, 5694.
[50] M. Gupta, K. K. Gleason, *Langmuir* **2006**, *22*, 10047.
[51] K. Chan, K. K. Gleason, *Langmuir* **2005**, *21*, 8930.
[52] G. Ozaydin-Ince, K. K. Gleason, *J. Vac. Sci. Technol. A* **2009**, *27*, 1135.
[53] J. R. Abelson, G. S. Girolami, *J. Vac. Sci. Technol. A* **2020**, *38*, 030802.
[54] W. E. Tenhaeff, K. K. Gleason, *Adv. Funct. Mater.* **2008**, *18*, 979.
[55] G. Ozaydin-Ince, J. M. Dubach, K. K. Gleason, H. A. Clark, *Proc. Natl. Acad. Sci. USA* **2011**, *108*, 2656.
[56] S. Nejati, K. K. S. Lau, *Nano Lett.* **2011**, *11*, 419.
[57] E. Ölçeroğlu, C.-Y. Hsieh, M. M. Rahman, K. K. S. Lau, M. McCarthy, *Langmuir* **2014**, *30*, 7556.
[58] V. V. Volkov, N. A. Platé, A. Takahara, T. Kajiyama, N. Amaya, Y. Murata, *Polymer* **1992**, *33*, 1316.
[59] G. de Crevoisier, P. Fabre, L. Leibler, S. Tencé-Girault, J. M. Corpart, *Macromolecules* **2002**, *35*, 3880.
[60] Y. Liu, Y. Higaki, M. Mukai, N. Ohta, T. Kabe, A. Takahara, *Polym. J.* **2019**, *51*, 189.
[61] S. Guan, W. Wen, Z. Yang, A. Chen, *Macromolecules* **2020**, *53*, 465.
[62] L. Shen, H. Guo, J. Zheng, X. Wang, Y. Yang, Z. An, *ACS Macro Lett.* **2018**, *7*, 287.
[63] M. Huo, D. Li, G. Song, J. Zhang, D. Wu, Y. Wei, J. Yuan, *Macromol. Rapid Commun.* **2018**, *39*, 1700840.
[64] L. Chen, W. Lu, C. M. Lieber, in *Semiconductor Nanowires: From Next-Generation Electronics to Sustainable Energy*, (Eds: W. Lu, J. Xiang), Royal Society of Chemistry, Cambridge **2015**, pp. 1–53.
[65] Y. Yu, L. Wu, J. Zhi, *Angew. Chem., Int. Ed.* **2014**, *53*, 14326.
[66] S. A. Fortuna, X. Li, *Semicond. Sci. Technol.* **2010**, *25*, 024005.
[67] R. S. Wagner, W. C. Ellis, *Appl. Phys. Lett.* **1964**, *4*, 89.
[68] W. A. Zisman, *Adv. Chem.* **1964**, *43*, 1.
[69] M. Huo, Y. Zhang, M. Zeng, L. Liu, Y. Wei, J. Yuan, *Macromolecules* **2017**, *50*, 8192.
[70] X. Li, B. Jin, Y. Gao, D. W. Hayward, M. A. Winnik, Y. Luo, I. Manners, *Angew. Chem., Int. Ed.* **2016**, *55*, 11392.